
Multi-approach gravity field models from Swarm GPS data

Signal and error in the Swarm models up to 2020-03-31

Delft University of Technology (TU Delft)
Astronomical Institute of the University of Bern (AIUB)
Astronomical Institute Ondřejov (ASU)
Institute of Geodesy Graz (IfG)
Ohio State University (OSU)

Version 1.0
2020-06-29

Prepared and checked by
João Encarnação
Work Package Manager

Approved by
Pieter Visser
Project Manager

Contents

1 Version history	5
2 Introduction	5
3 Source data	5
4 Methodology	6
4.1 Combination	6
4.2 Validation	6
5 Results	9
5.1 Spatial analysis	9
5.2 Temporal analysis	12
5.3 Time series of storage catchments	15
5.4 Temporal variability	33
References	34

List of Figures

1 Monthly (GSFC) and weekly (GSFC-7DAY) versions of the time series of Satellite Laser Ranging (SLR)-derived C_{20} from Loomis, Rachlin and Luthcke (2019), compared to Cheng and Ries (2018) (TN-11) and Loomis and Rachlin (2020) (TN-14).	7
2 Deep ocean mask.	7
3 Temporal variability of the Gravity Recovery And Climate Experiment (GRACE)/ GRACE Follow On (GRACE-FO) climatological model, including the boundaries of the regions analysed in Section 5.3.1 to Section 5.3.18.	8
4 Per-degree mean of the RMS difference (top) and cumulative degree-mean temporal RMS difference (bottom) between the Swarm Gravity Field Models (GFMs) and GRACE-based prediction, considering 750km Gaussian smoothing. This is (an estimate of) the average per-degree quality of the various Swarm solutions in the spectral domain (top) and globally (bottom) . The degree amplitudes remain relatively constant with increasing degree, instead of growing in terms of Equivalent Water Height (EWH), as the result of the smoothing.	9
5 Epoch-wise cumulative spatial RMS (top) and its global average (bottom) of the difference between Swarm GFMs and GRACE-based prediction, over land areas, considering 750km Gaussian smoothing. This is (an estimate of) the evolution of the ability of the various Swarm solutions to predict land mass transport processes over time (top) and its global sum (bottom).	10
6 Epoch-wise cumulative spatial RMS (top) and its global sum (bottom) of the difference between Swarm GFMs and GRACE-based prediction, over ocean areas, considering 750km Gaussian smoothing. This is the epoch-wise quality of the Swarm GFMs, and reported in the header of the combined GFMs files.	11

7	Per-degree mean (top) and its overall cumulative (bottom) of the correlation coefficient between Swarm GFM ^s and GRACE-based prediction, over land areas, considering 750km Gaussian smoothing. The temporal correlation at every Stokes coefficient is computed and the average over each degree is plotted at the top. It illustrates how well the temporal variations of the Swarm models agree with what is predicted from the GRACE/GRACE-FO climatological model.	12
8	Per-degree mean (top) and its overall cumulative (bottom) of the correlation coefficient between Swarm GFM ^s and GRACE-based prediction, over ocean areas, considering 750km Gaussian smoothing. It illustrates that the Swarm models agree poorly with the mass variations over the ocean as predicted by the GRACE/GRACE-FO climatological model.	13
9	Per-coefficient RMS difference between Swarm GFM ^s and GRACE-based prediction considering 750km Gaussian smoothing, over land (left column) and ocean (right column) areas, for AIUB, ASU, IfG, OSU and combined solutions (respectively from top to bottom).	14
10	Time series of EWH for the Amazon basin (latitude -17 to 3 degrees, longitude -76 to -47 degrees).	15
11	Time series of EWH for the Orinoco basin (latitude -3 to 12 degrees, longitude -72 to -59 degrees).	16
12	Time series of EWH for the La Plata basin (latitude -34 to -19 degrees, longitude -65 to -50 degrees).	17
13	Time series of EWH for the Mississippi basin (latitude 29 to 44 degrees, longitude -101 to -80 degrees).	18
14	Time series of EWH for the Columbia region (latitude 38 to 50 degrees, longitude -125 to -110 degrees).	19
15	Time series of EWH for the Alaska (latitude 56 to 65 degrees, longitude -151 to -129 degrees).	20
16	Time series of EWH for the Western Greenland region (latitude 60 to 85 degrees, longitude -60 to -37 degrees).	21
17	Time series of EWH for the Danube basin (latitude 43 to 48 degrees, longitude 13 to 28 degrees).	22
18	Time series of EWH for the Western Sub-Saharan basin (latitude 5 to 15 degrees, longitude -15 to -1 degrees).	23
19	Time series of EWH for the Eastern Sub-Saharan basin (latitude 1 to 13 degrees, longitude -8 to 35 degrees).	24
20	Time series of EWH for the Congo and Zambezi basins (latitude -23 to -3 degrees, longitude 14 to 38 degrees).	25
21	Time series of EWH for the Volga basin (latitude 53 to 61 degrees, longitude 34 to 56 degrees).	26
22	Time series of EWH for the Siberia region (latitude 57 to 72 degrees, longitude 68 to 109 degrees).	27
23	Time series of EWH for the Ganges-Brahmaputra basin (latitude 15 to 30 degrees, longitude 72 to 89 degrees).	28
24	Time series of EWH for the Indochina region (latitude 12 to 29 degrees, longitude 93 to 105 degrees).	29
25	Time series of EWH for the Northern Australia region (latitude -24 to -10 degrees, longitude 124 to 145 degrees).	30
26	Time series of EWH for the Western Antarctica region (latitude -80 to -70 degrees, longitude -140 to -85 degrees).	31

27	Time series of EWH for the Eastern Antarctica region (latitude -80 to -68 degrees, longitude 80 to 130 degrees)	32
28	Temporal variability of the Swarm combined solutions and	33

List of Tables

1	Overview of the gravity field estimation approaches	5
2	Versions of the GFMs, and the Kinematic Orbits (KOs) used in their estimation, relevant to this report.	6
3	Statistics of the agreement between GRACE/GRACE-FO and Swarm time series relative to the GRACE/GRACE-FO climatological model for the Amazon basin. .	15
4	Statistics of the agreement between GRACE/GRACE-FO and Swarm time series relative to the GRACE/GRACE-FO climatological model for the Orinoco basin. .	16
5	Statistics of the agreement between GRACE/GRACE-FO and Swarm time series relative to the GRACE/GRACE-FO climatological model for the La Plata basin. .	17
6	Statistics of the agreement between GRACE/GRACE-FO and Swarm time series relative to the GRACE/GRACE-FO climatological model for the Mississippi basin. .	18
7	Statistics of the agreement between GRACE/GRACE-FO and Swarm time series relative to the GRACE/GRACE-FO climatological model for the Columbia region. .	19
8	Statistics of the agreement between GRACE/GRACE-FO and Swarm time series relative to the GRACE/GRACE-FO climatological model for the Alaska.	20
9	Statistics of the agreement between GRACE/GRACE-FO and Swarm time series relative to the GRACE/GRACE-FO climatological model for the Western Green-land region.	21
10	Statistics of the agreement between GRACE/GRACE-FO and Swarm time series relative to the GRACE/GRACE-FO climatological model for the Danube basin. .	22
11	Statistics of the agreement between GRACE/GRACE-FO and Swarm time series relative to the GRACE/GRACE-FO climatological model for the Western Sub-Saharan basin.	23
12	Statistics of the agreement between GRACE/GRACE-FO and Swarm time series relative to the GRACE/GRACE-FO climatological model for the Eastern Sub-Saharan basin.	24
13	Statistics of the agreement between GRACE/GRACE-FO and Swarm time series relative to the GRACE/GRACE-FO climatological model for the Congo and Zambezi basins.	25
14	Statistics of the agreement between GRACE/GRACE-FO and Swarm time series relative to the GRACE/GRACE-FO climatological model for the Volga basin. . .	26
15	Statistics of the agreement between GRACE/GRACE-FO and Swarm time series relative to the GRACE/GRACE-FO climatological model for the Siberia region. .	27
16	Statistics of the agreement between GRACE/GRACE-FO and Swarm time series relative to the GRACE/GRACE-FO climatological model for the Ganges-Brahmaputra basin.	28
17	Statistics of the agreement between GRACE/GRACE-FO and Swarm time series relative to the GRACE/GRACE-FO climatological model for the Indochina region. .	29
18	Statistics of the agreement between GRACE/GRACE-FO and Swarm time series relative to the GRACE/GRACE-FO climatological model for the Northern Aus-tralia region.	30

19	Statistics of the agreement between GRACE/GRACE-FO and Swarm time series relative to the GRACE/GRACE-FO climatological model for the Western Antarctica region.	31
20	Statistics of the agreement between GRACE/GRACE-FO and Swarm time series relative to the GRACE/GRACE-FO climatological model for the Eastern Antarctica region.	32
21	Statistics of the agreement between the GRACE and Swarm time series for the regions displayed in Sections Section 5.3.1 to Section 5.3.18.	33

1 Version history

Version 1, 2020-06-29

- Validation of combined models version 09, from start of mission until 2020-03-31.

2 Introduction

We report some statistics of the individual and combined GFMs produced on the context of the *Multi-approach gravity field models from Swarm GPS data* project. The approach for combining individual gravity field solutions, i.e. those produced by the various partners mentioned in Section 3, is described in Section 4.1. The procedure and assumption used to derive the statistics is described in Section 4.2. Finally, the results are presented in Section 5.

This report does not intend to draw conclusions regarding the presented statistics, it is merely a descriptive document of the signal and error in the individual and combined Swarm GFMs. For this reason, the text in Section 5 is restricted to clarifying the quantities shown in the plots.

3 Source data

The individual gravity field solutions are produced by the institutes listed in Table 1.

Table 1 – Overview of the gravity field estimation approaches

Inst.	Approach	Reference
AIUB	Celestial Mechanics Approach (Beutler et al., 2010)	Jäggi et al. (2016)
ASU	Decorrelated Acceleration Approach (Bezděk et al., 2014; Bezděk et al., 2016)	Bezděk et al. (2016)
IfG	Short-Arcs Approach (Mayer-Gürr, 2006)	Zehentner and Mayer-Gürr (2016)
OSU	Improved Energy Balance Approach (Shang et al., 2015)	Guo et al. (2015)

Additional details about the different gravity field approaches can be found in (Teixeira da Encarnação and Visser, 2017).

The version of the individual GFMs is listed in Table 2.

The version numbers listed in Table 2 are relevant within the project and are reported so that it is possible to trace back the results presented in Section 5. Particular to the combined models, version 09 relates to the chosen combination strategy, as concluded from Teixeira da Encarnação and Visser (2019).

Gravity Field Model	version	Kinematic Orbit
AIUB	01	AIUB
ASU	02	IfG
IfG	03 – 06	IfG
OSU	02	AIUB
combined	09	N/A

Table 2 – Versions of the GFMs, and the KOs used in their estimation, relevant to this report.

4 Methodology

4.1 Combination

The combination of the models is conducted at the level of the solutions considering weights derived from Variance Component Estimation (VCE). As demonstrated in Teixeira da Encarnação and Visser (2019), the combination at the level of Normal Equation (NEQ) disagreed more with GRACE/GRACE-FO, as a result of the vastly different amplitudes of formal errors.

The combination considers the complete degree range (degrees 2 to 40) but the VCE weights are derived from degrees 2-20. This approach addresses the very high errors above degree 20, which would otherwise drive the value of the weights.

It is feasible to determine the VCE weights because there are two time-series based on AIUB orbits (i.e. AIUB and OSU) and two time-series based on IfG orbits (i.e. IfG and ASU). Therefore the impact of the KOs on the solutions and on the VCE weights is balanced.

4.2 Validation

The validation is done by comparing the individual and combined solutions to a model estimated from the Release 6 (RL06) GRACE/GRACE-FO GFMs produced at Center for Space Research (CSR), considering all solutions available at the this document is produced. This models fits a degree 1 polynomial and a yearly, semi-yearly, S2, K1 and K2 periods to the GRACE/GRACE-FO time series; the time series produced on the basis of the parameters resulting from this regression are referred to as *GRACE/GRACE-FO climatological model*.

The $C_{2,0}$ coefficient in all solutions has been replaced by the weekly time series provided by Goddard Space Flight Center (GSFC) (Loomis, Rachlin and Luthcke, 2019).

All solutions undergo a 750km radius spherical cap Gaussian filtering, unless otherwise noted, to clearly show the geophysical signal contained in the Swarm solutions. The GRACE and GOCE Gravity Model 05 (GGM05G) (Bettadpur et al., 2015) static GFM is subtracted from all models in order to isolate the time-variable component of Earth's gravity field. We chose to show the gravity field in terms of EWH, except for the statistics related to the correlation coefficient, which are non-dimensional as usual. The GRACE/GRACE-FO gravity field time series is linearly interpolated to the mid-month epoch of the Swarm solutions. The GRACE/GRACE-FO climatological model is evaluated at the same time domain. The analysis spans the complete Swarm mission period until 2020-03-31.

Some analyses are restricted to either the land or ocean areas. In those cases, the land or ocean mask is applied in the spatial domain and a Spherical Harmonic (SH) analysis is done on the masked grid. The ocean mask excludes the coastal ocean areas that are roughly 1000km or less from land areas, as shown in Figure 2, while the land mask has no buffer zone.

In Section 5.3, the geophysical signal represented by the Swarm solutions is evaluated on the basis of the time series of average EWH over restricted geographical locations, shown in Figure 3.

Multi-approach gravity field models from Swarm GPS data

SW_VR_DUT_GS_0005] version 1.0

2020-06-29

Page 7 of 36

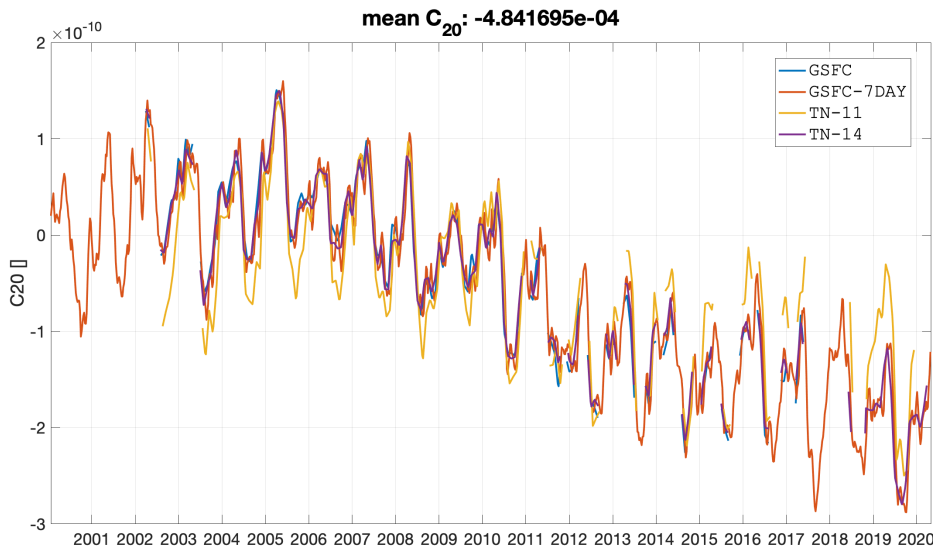


Figure 1 – Monthly (GSFC) and weekly (GSFC-7DAY) versions of the time series of SLR-derived C_{20} from Loomis, Rachlin and Luthcke (2019), compared to Cheng and Ries (2018) (TN-11) and Loomis and Rachlin (2020) (TN-14).

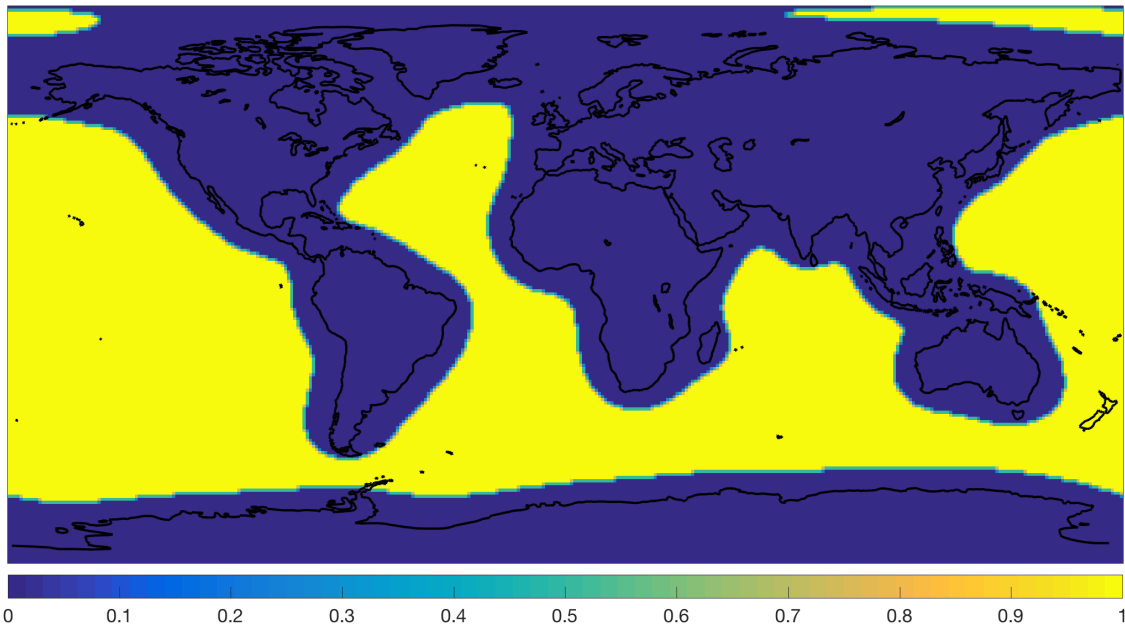


Figure 2 – Deep ocean mask.

Each averaging is done over the corresponding spatial truncation of an equiangular grid representation of the SH coefficients. The locations shown in Sections 5.3.1 to 5.3.18 are related to the largest hydrological basins and polar regions with the highest signal variability observed by GRACE/GRACE-FO. Note that there is no effort to meticulously consider or implement proper leakage reduction methods, e.g. by Guo, Duan and Shum (2010). We perform a parametric regression on all time series considering a constant and drift terms,

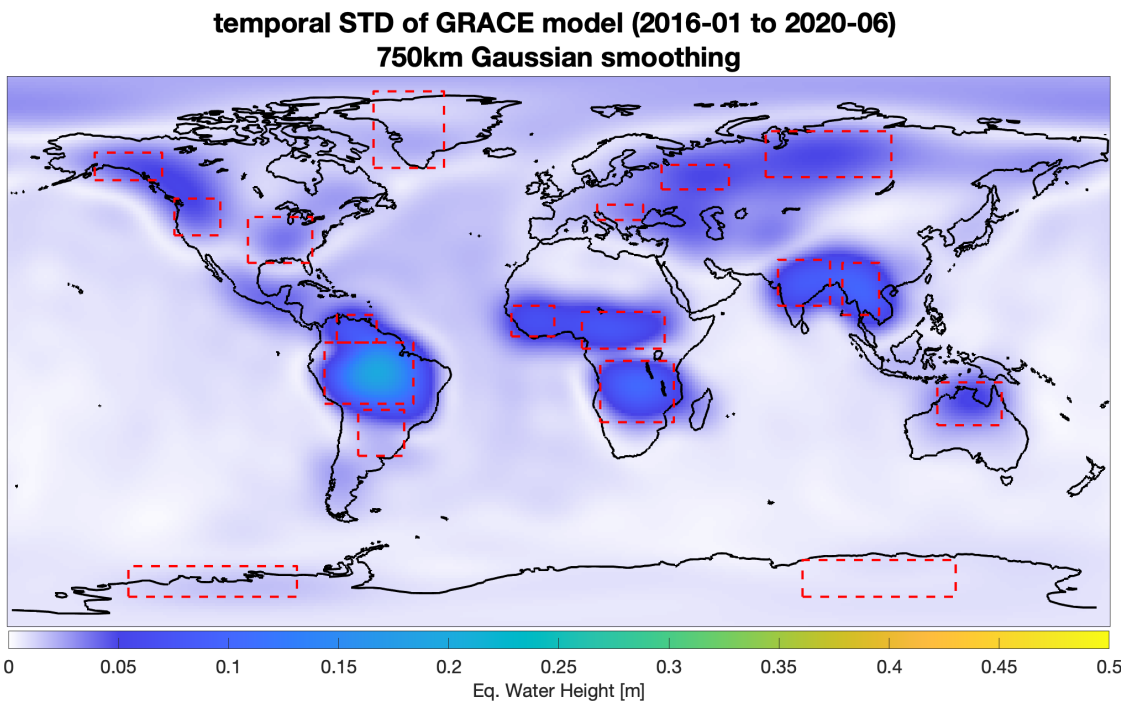


Figure 3 – Temporal variability of the GRACE/GRACE-FO climatological model, including the boundaries of the regions analysed in Section 5.3.1 to Section 5.3.18.

along with annual and semi-annual sine and co-sine terms to improve the robustness. We plot the linear part of this regression, in order to quantify the accuracy of Swarm-derived climatological trends. The time series are plotted along with tables presenting some statistics. The values of the constant and linear terms for the Swarm and GRACE/GRACE-FO solutions (column 1) are show in terms of EWH (columns 2 and 4). Additionally, the difference of these parameters between the Swarm and GRACE/GRACE-FO solutions relative to the GRACE/GRACE-FO climatological model is listed in columns 3 and 5 (the values for the latter data set in these columns is zero). Finally, the correlation coefficients is presented in the last column (the value for GRACE/GRACE-FO climatological model is 1). The constant term is the average basin storage over the relevant data period.

5 Results

5.1 Spatial analysis

5.1.1 Degree-mean RMS difference

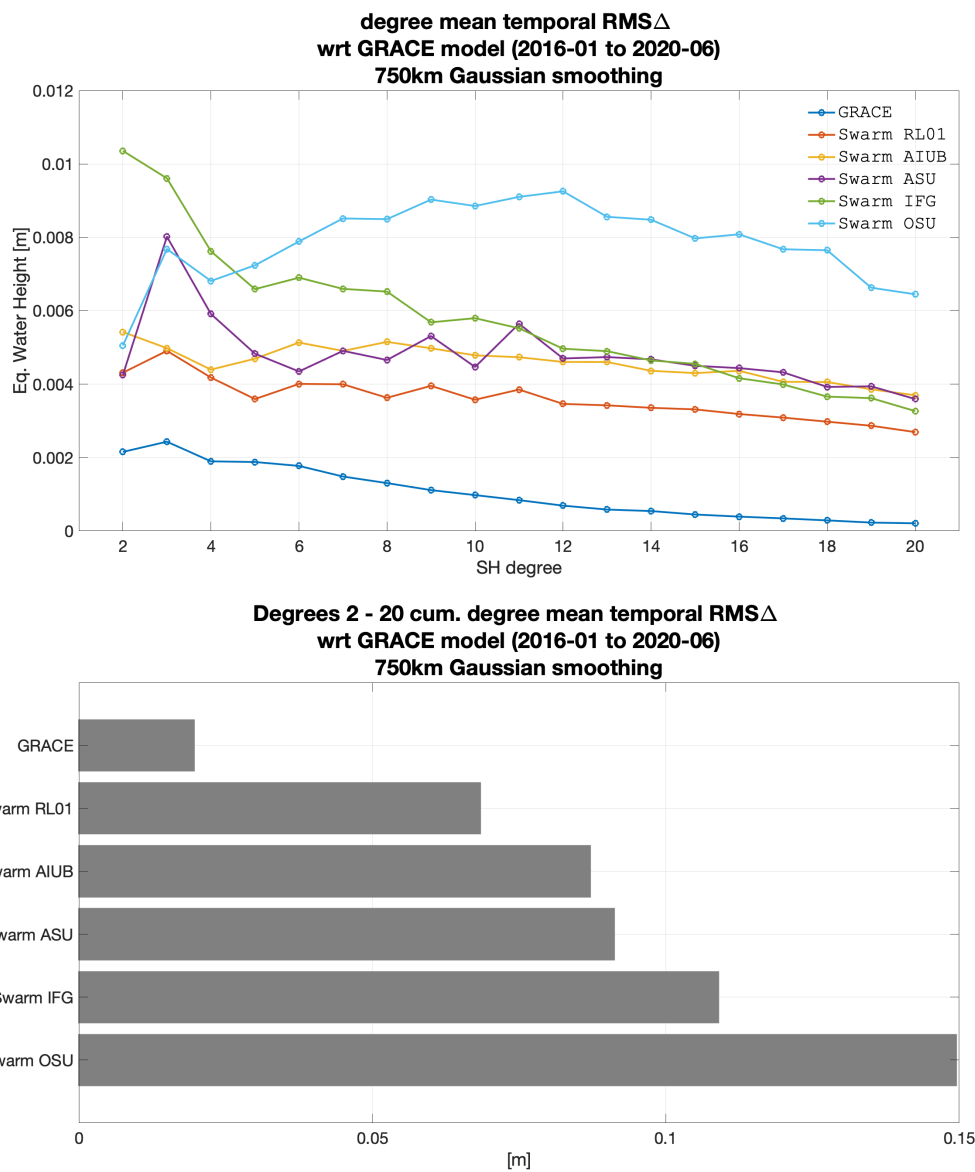


Figure 4 – Per-degree mean of the RMS difference (top) and cumulative degree-mean temporal RMS difference (bottom) between the Swarm GFMs and GRACE-based prediction, considering 750km Gaussian smoothing. This is (an estimate of) the average per-degree quality of the various Swarm solutions in the spectral domain (top) and globally (bottom). The degree amplitudes remain relatively constant with increasing degree, instead of growing in terms of EWH, as the result of the smoothing.

5.1.2 Cumulative degree amplitude difference over land

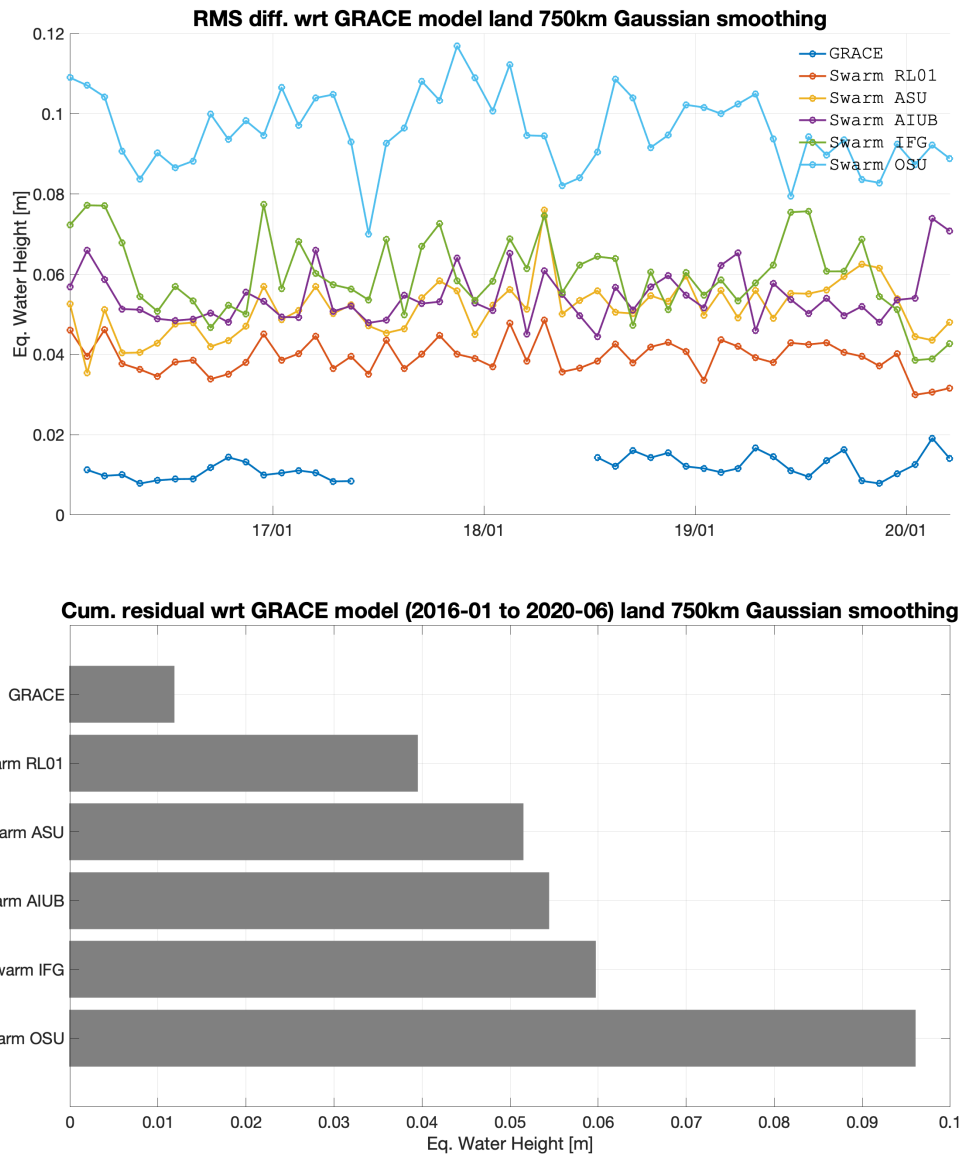


Figure 5 – Epoch-wise cumulative spatial RMS (top) and its global average (bottom) of the difference between Swarm GFMs and GRACE-based prediction, over land areas, considering 750km Gaussian smoothing. This is (an estimate of) the evolution of the ability of the various Swarm solutions to predict land mass transport processes over time (top) and its global sum (bottom).

5.1.3 Cumulative degree amplitude difference over oceans

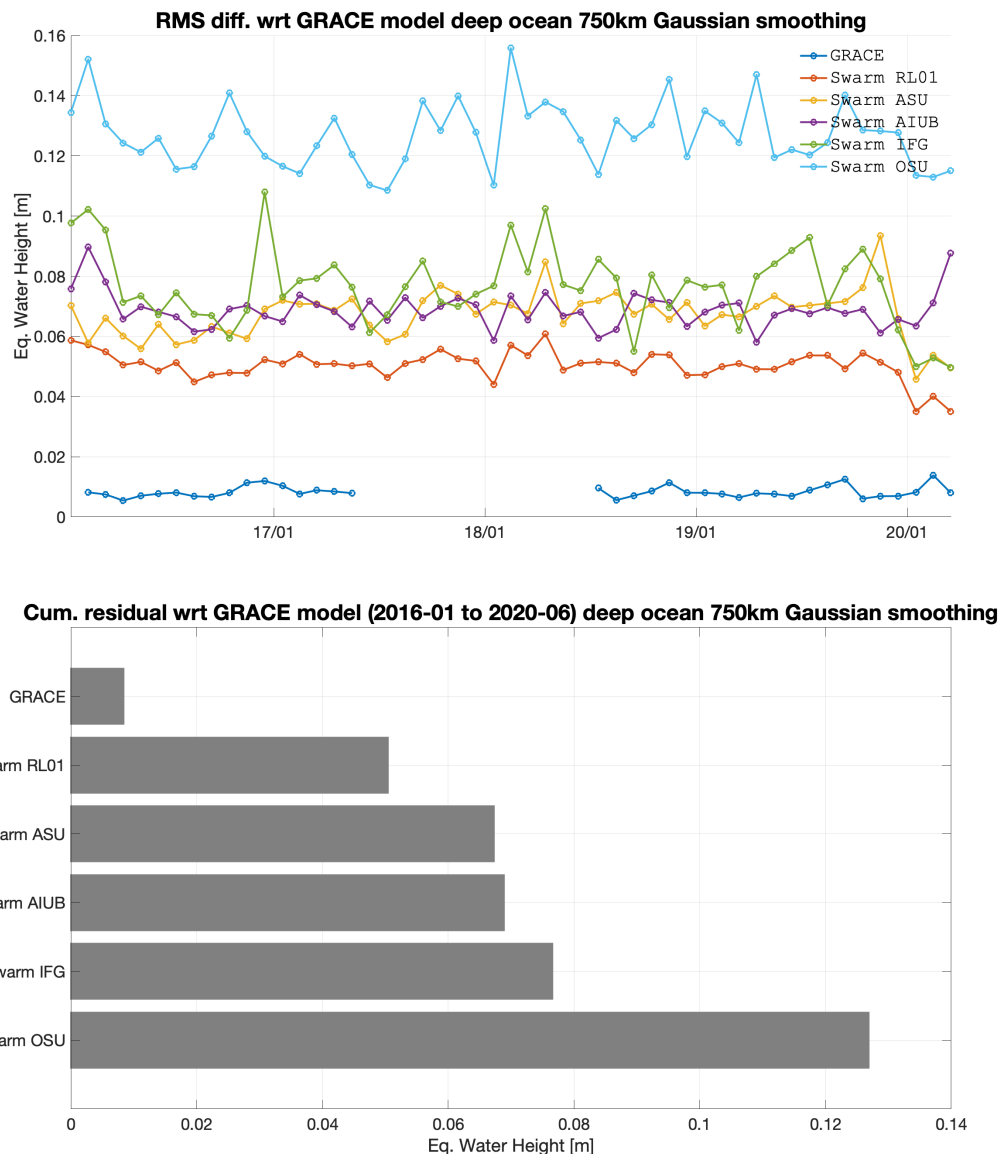


Figure 6 – Epoch-wise cumulative spatial RMS (top) and its global sum (bottom) of the difference between Swarm GFMs and GRACE-based prediction, over ocean areas, considering 750km Gaussian smoothing. This is the epoch-wise quality of the Swarm GFMs, and reported in the header of the combined GFMs files.

5.2 Temporal analysis

5.2.1 Cumulative degree amplitude difference over land

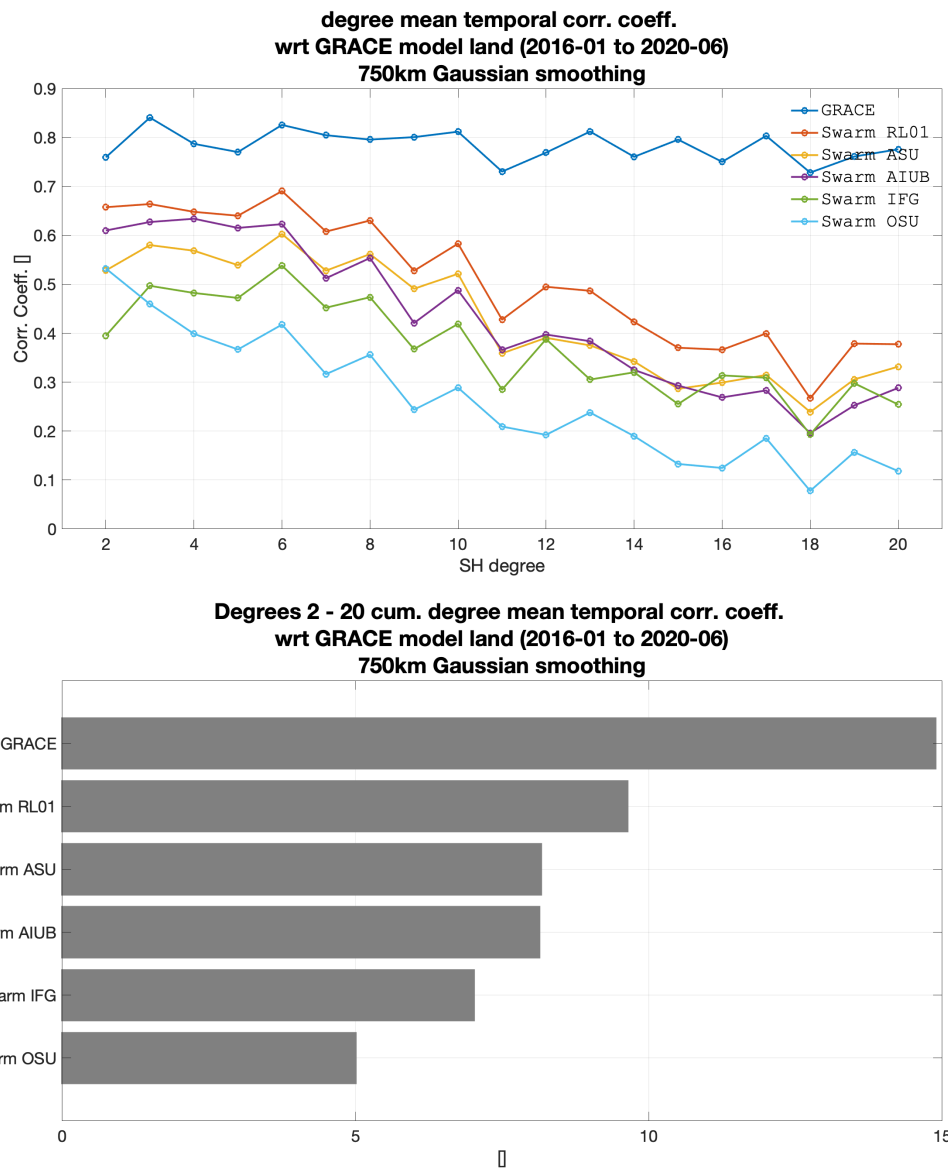


Figure 7 – Per-degree mean (top) and its overall cumulative (bottom) of the correlation coefficient between Swarm GFMs and GRACE-based prediction, over land areas, considering 750km Gaussian smoothing. The temporal correlation at every Stokes coefficient is computed and the average over each degree is plotted at the top. It illustrates how well the temporal variations of the Swarm models agree with what is predicted from the GRACE/GRAVE-FO climatological model.

5.2.2 Cumulative degree amplitude difference over oceans

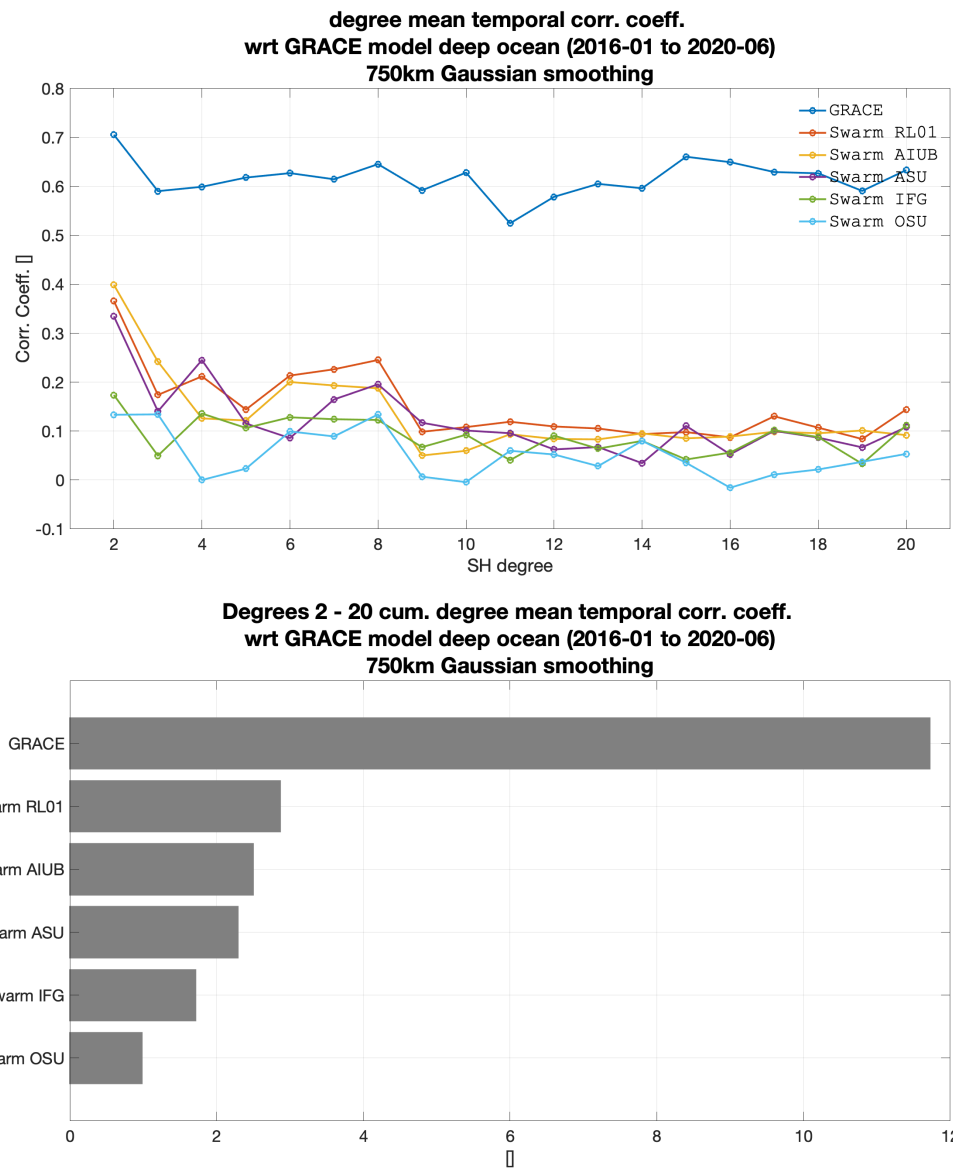


Figure 8 – Per-degree mean (top) and its overall cumulative (bottom) of the correlation coefficient between Swarm GFM and GRACE-based prediction, over ocean areas, considering 750km Gaussian smoothing. It illustrates that the Swarm models agree poorly with the mass variations over the ocean as predicted by the GRACE/GRAVE-FO climatological model.

5.2.3 Triangular plots of the RMS differences

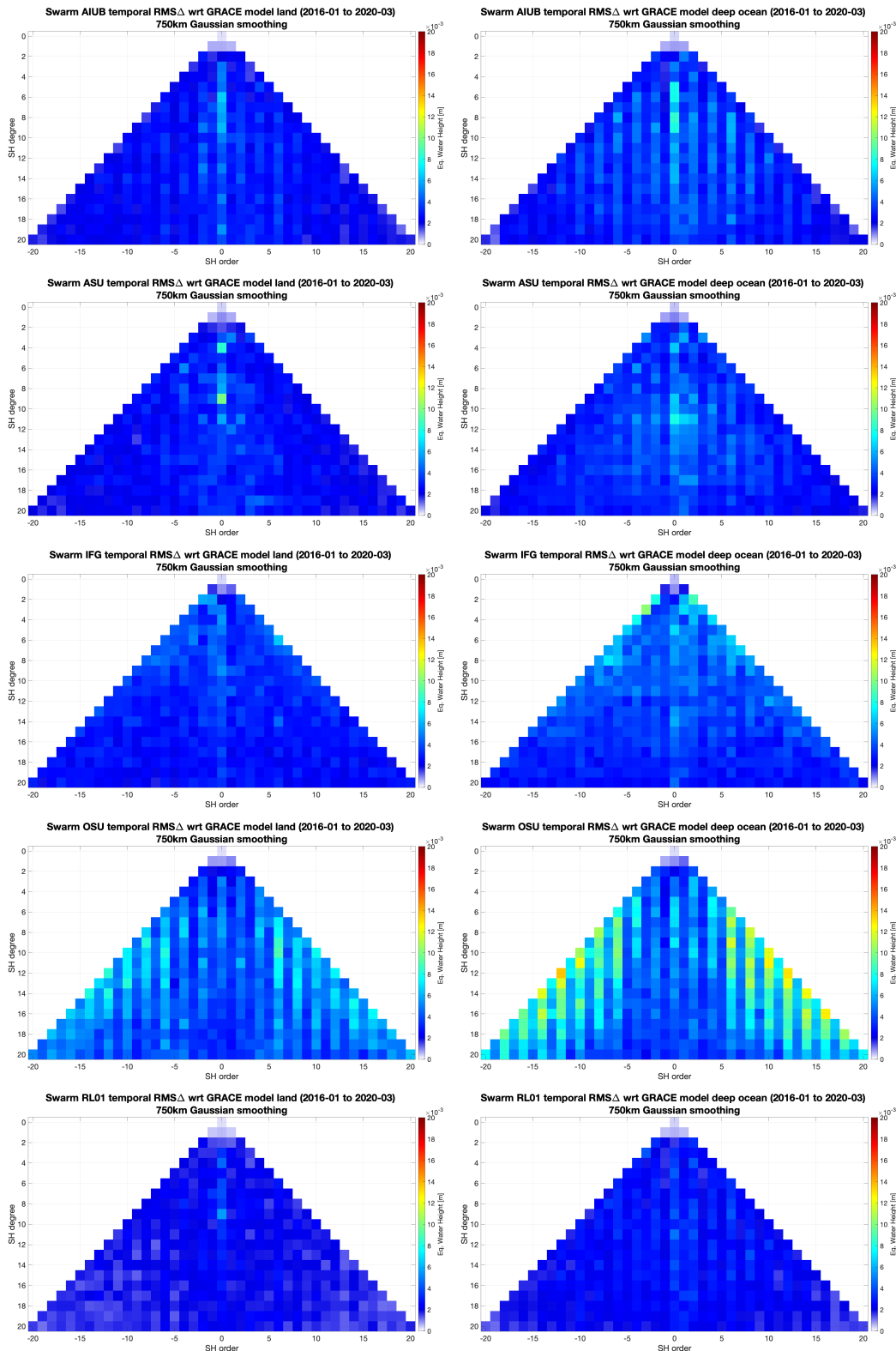


Figure 9 – Per-coefficient RMS difference between Swarm GFMs and GRACE-based prediction considering 750km Gaussian smoothing, over land (left column) and ocean (right column) areas, for AIUB, ASU, IfG, OSU and combined solutions (respectively from top to bottom).

5.3 Time series of storage catchments

5.3.1 Amazon basin

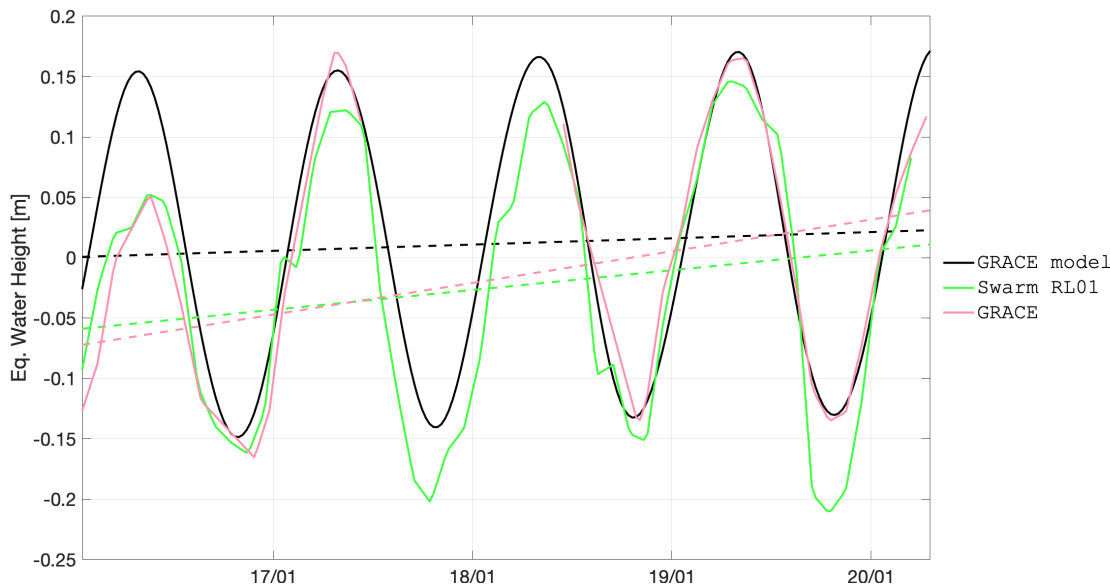


Figure 10 – Time series of EWH for the Amazon basin (latitude -17 to 3 degrees, longitude -76 to -47 degrees).

solution	constant term [cm]	constant term Δ [cm]	linear term [cm/year]	linear term Δ [cm/year]	corr. coeff. []
GRACE MODEL	2.16	0.00	0.52	0.00	1.00
Swarm RL01	-2.20	-4.36	1.64	1.12	0.95
GRACE	1.08	-1.08	2.62	2.10	0.91

Table 3 – Statistics of the agreement between GRACE/GRACE-FO and Swarm time series relative to the GRACE/GRACE-FO climatological model for the Amazon basin.

5.3.2 Orinoco basin

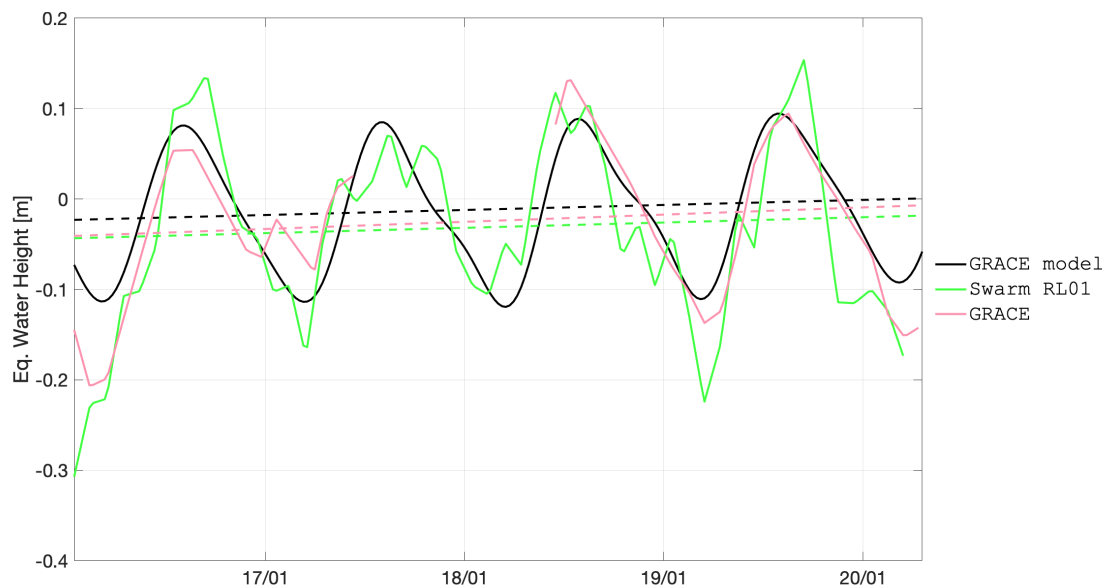


Figure 11 – Time series of EWH for the Orinoco basin (latitude -3 to 12 degrees, longitude -72 to -59 degrees).

solution	constant term [cm]	constant term Δ [cm]	linear term [cm/year]	linear term Δ [cm/year]	corr. coeff. []
GRACE MODEL	-1.59	0.00	0.56	0.00	1.00
Swarm RL01	-3.81	-2.23	0.59	0.03	0.83
GRACE	-3.47	-1.88	0.80	0.24	0.90

Table 4 – Statistics of the agreement between GRACE/GRACE-FO and Swarm time series relative to the GRACE/GRACE-FO climatological model for the Orinoco basin.

5.3.3 La Plata basin

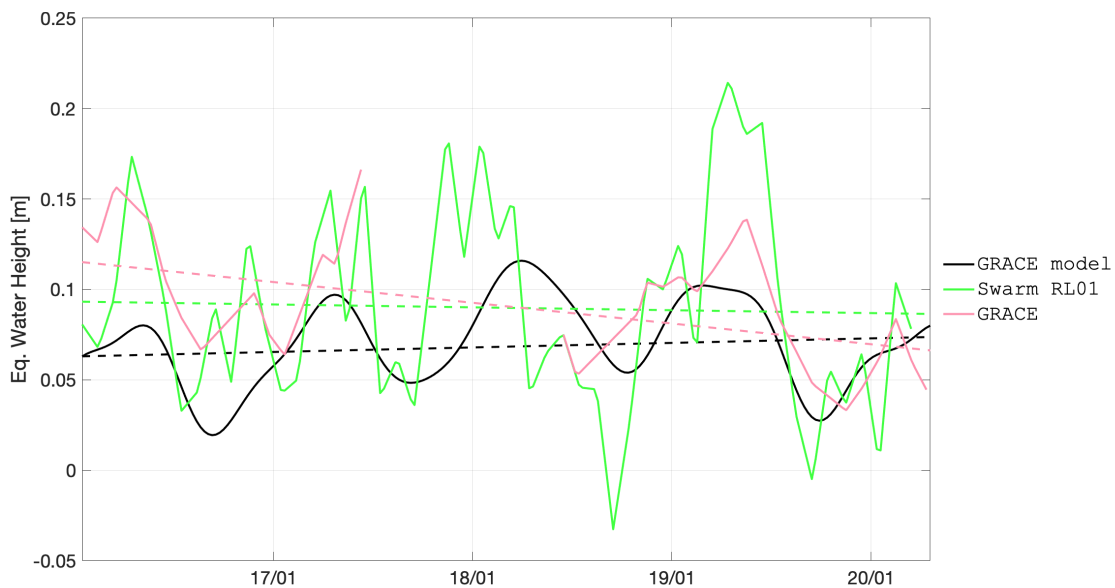


Figure 12 – Time series of EWH for the La Plata basin (latitude -34 to -19 degrees, longitude -65 to -50 degrees).

solution	constant term [cm]	constant term Δ [cm]	linear term [cm/year]	linear term Δ [cm/year]	corr. coeff. []
GRACE MODEL	7.04	0.00	0.25	0.00	1.00
Swarm RL01	9.05	2.01	-0.16	-0.41	0.52
GRACE	9.32	2.28	-1.15	-1.40	0.54

Table 5 – Statistics of the agreement between GRACE/GRACE-FO and Swarm time series relative to the GRACE/GRACE-FO climatological model for the La Plata basin.

5.3.4 Mississippi basin

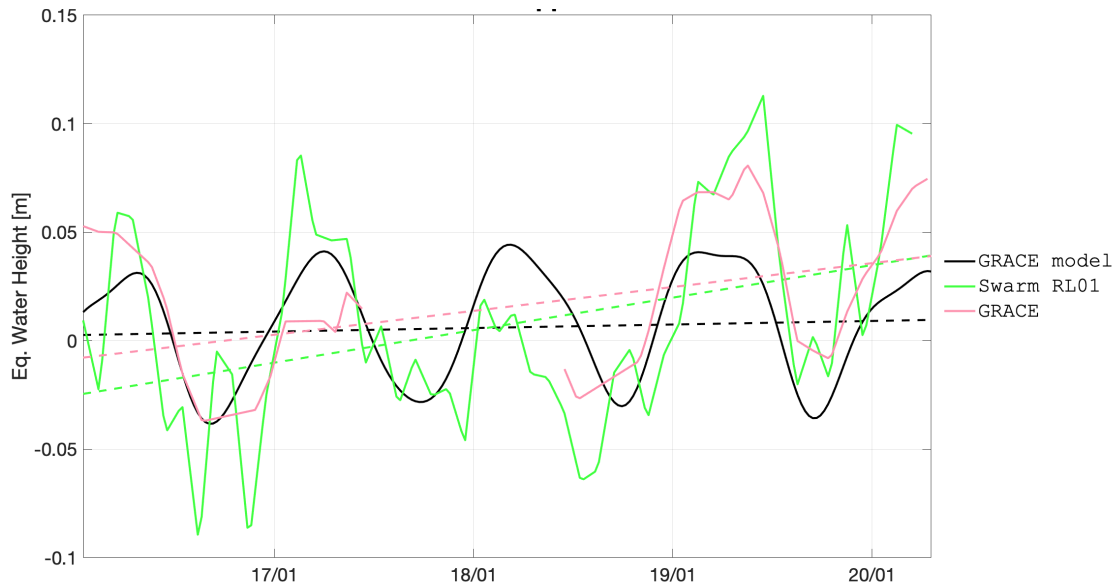


Figure 13 – Time series of EWH for the Mississippi basin (latitude 29 to 44 degrees, longitude -101 to -80 degrees).

solution	constant term [cm]	constant term Δ [cm]	linear term [cm/year]	linear term Δ [cm/year]	corr. coeff. []
GRACE MODEL	0.86	0.00	0.16	0.00	1.00
Swarm RL01	0.88	0.01	1.50	1.34	0.62
GRACE	2.52	1.66	1.10	0.94	0.78

Table 6 – Statistics of the agreement between GRACE/GRACE-FO and Swarm time series relative to the GRACE/GRACE-FO climatological model for the Mississippi basin.

5.3.5 Columbia region

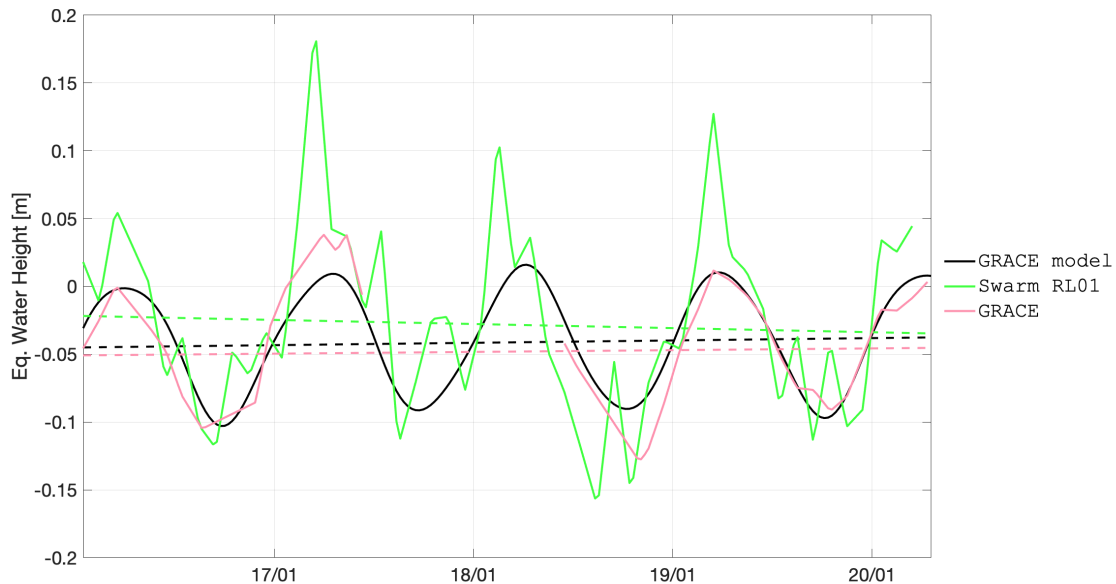


Figure 14 – Time series of EWH for the Columbia region (latitude 38 to 50 degrees, longitude -125 to -110 degrees).

solution	constant term [cm]	constant term Δ [cm]	linear term [cm/year]	linear term Δ [cm/year]	corr. coeff. []
GRACE MODEL	-3.75	0.00	0.17	0.00	1.00
Swarm RL01	-2.41	1.34	-0.30	-0.48	0.78
GRACE	-3.80	-0.05	0.13	-0.04	0.93

Table 7 – Statistics of the agreement between GRACE/GRACE-FO and Swarm time series relative to the GRACE/GRACE-FO climatological model for the Columbia region.

5.3.6 Alaska

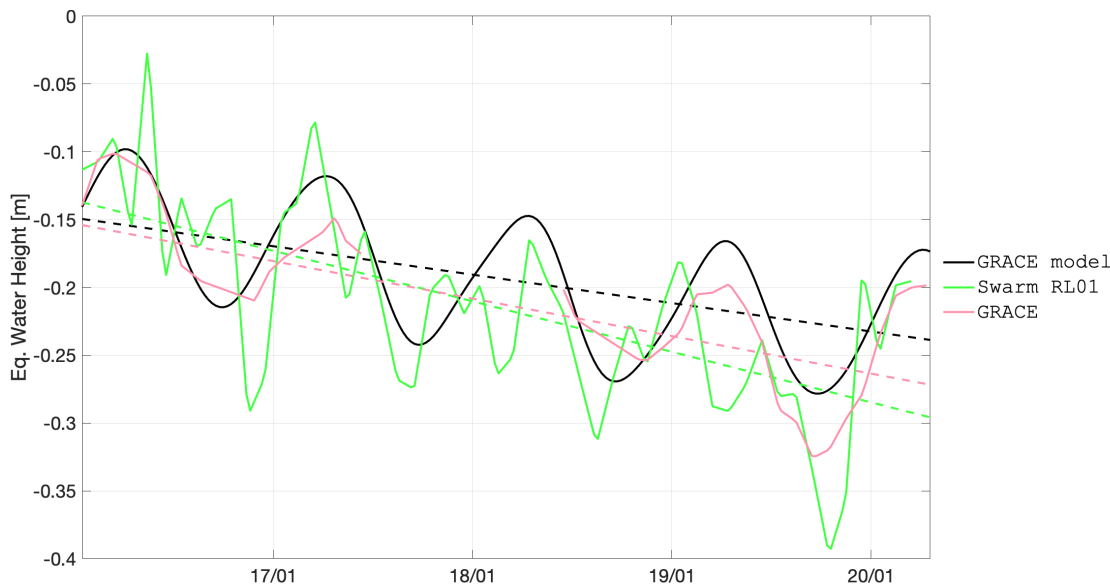


Figure 15 – Time series of EWH for the Alaska (latitude 56 to 65 degrees, longitude -151 to -129 degrees).

solution	constant term [cm]	constant term Δ [cm]	linear term [cm/year]	linear term Δ [cm/year]	corr. coeff. []
GRACE MODEL	-19.18	0.00	-2.10	0.00	1.00
Swarm RL01	-21.27	-2.10	-3.73	-1.63	0.73
GRACE	-20.94	-1.76	-2.77	-0.67	0.93

Table 8 – Statistics of the agreement between GRACE/GRACE-FO and Swarm time series relative to the GRACE/GRACE-FO climatological model for the Alaska.

5.3.7 Western Greenland region

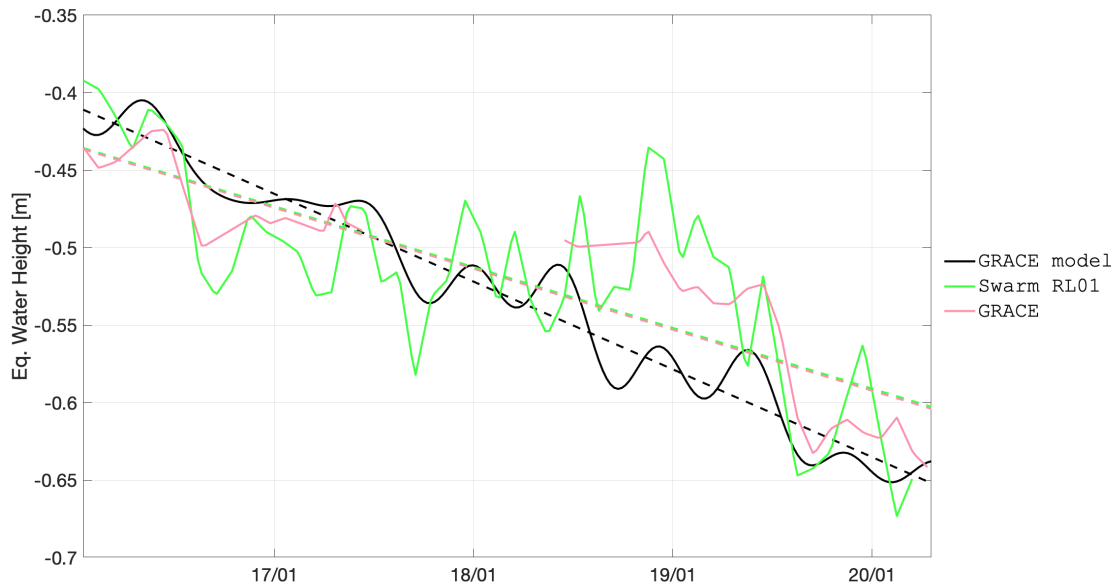


Figure 16 – Time series of EWH for the Western Greenland region (latitude 60 to 85 degrees, longitude -60 to -37 degrees).

solution	constant term [cm]	constant term Δ [cm]	linear term [cm/year]	linear term Δ [cm/year]	corr. coeff. []
GRACE MODEL	-53.47	0.00	-5.66	0.00	1.00
Swarm RL01	-51.70	1.78	-3.92	1.74	0.77
GRACE	-52.37	1.10	-3.93	1.73	0.91

Table 9 – Statistics of the agreement between GRACE/GRACE-FO and Swarm time series relative to the GRACE/GRACE-FO climatological model for the Western Greenland region.

5.3.8 Danube basin

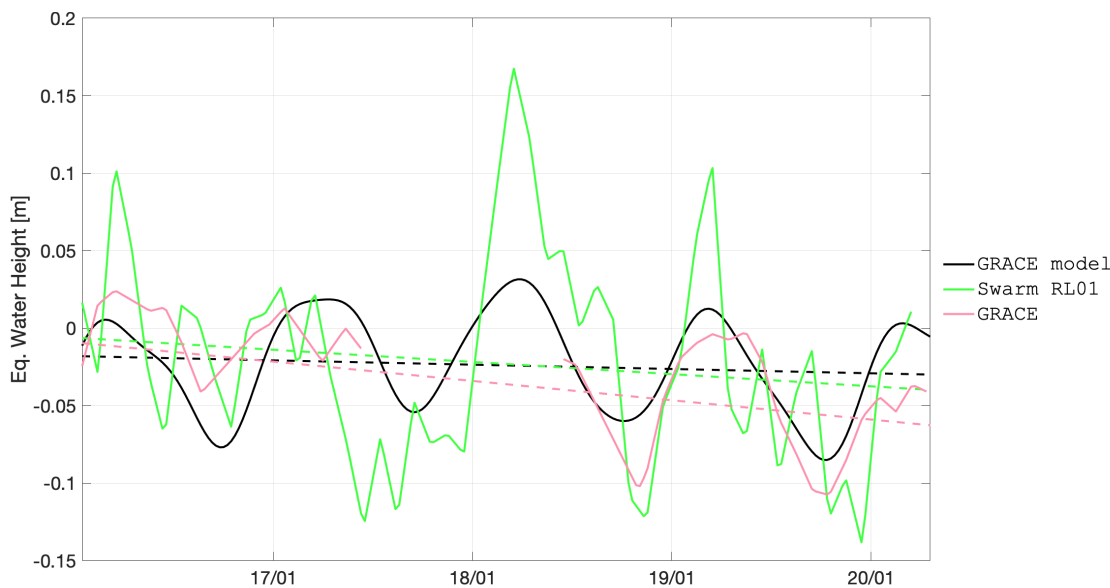


Figure 17 – Time series of EWH for the Danube basin (latitude 43 to 48 degrees, longitude 13 to 28 degrees).

solution	constant term [cm]	constant term Δ [cm]	linear term [cm/year]	linear term Δ [cm/year]	corr. coeff. []
GRACE MODEL	-2.14	0.00	-0.28	0.00	1.00
Swarm RL01	-1.92	0.22	-0.79	-0.51	0.57
GRACE	-3.04	-0.90	-1.25	-0.97	0.70

Table 10 – Statistics of the agreement between GRACE/GRACE-FO and Swarm time series relative to the GRACE/GRACE-FO climatological model for the Danube basin.

5.3.9 Western Sub-Saharan basin

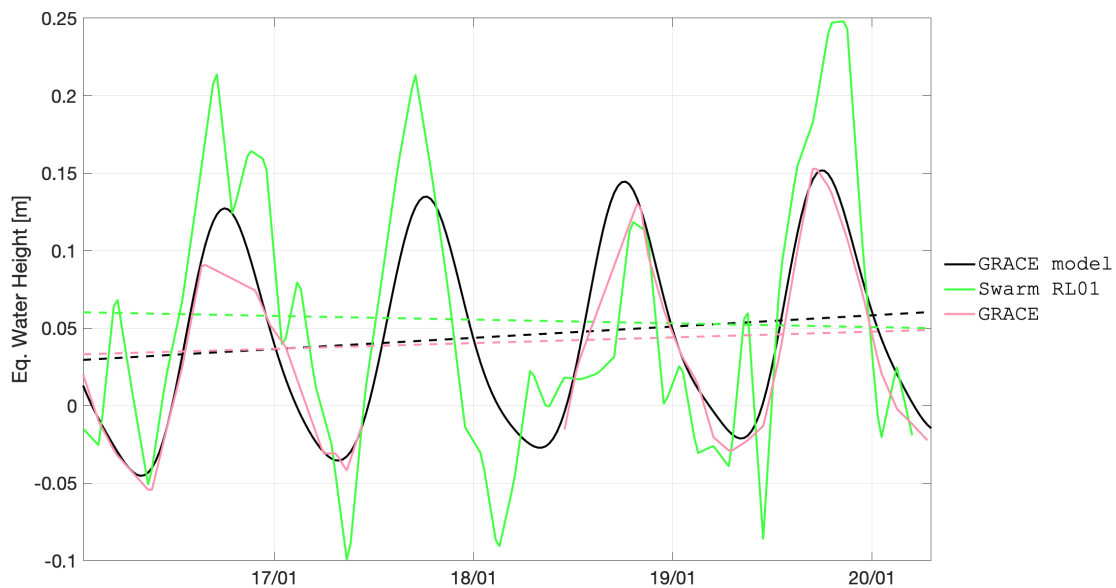


Figure 18 – Time series of EWH for the Western Sub-Saharan basin (latitude 5 to 15 degrees, longitude -15 to -1 degrees).

solution	constant term [cm]	constant term Δ [cm]	linear term [cm/year]	linear term Δ [cm/year]	corr. coeff. []
GRACE MODEL	3.99	0.00	0.73	0.00	1.00
Swarm RL01	5.16	1.17	-0.24	-0.97	0.79
GRACE	2.64	-1.35	0.37	-0.36	0.98

Table 11 – Statistics of the agreement between GRACE/GRACE-FO and Swarm time series relative to the GRACE/GRACE-FO climatological model for the Western Sub-Saharan basin.

5.3.10 Eastern Sub-Saharan basin

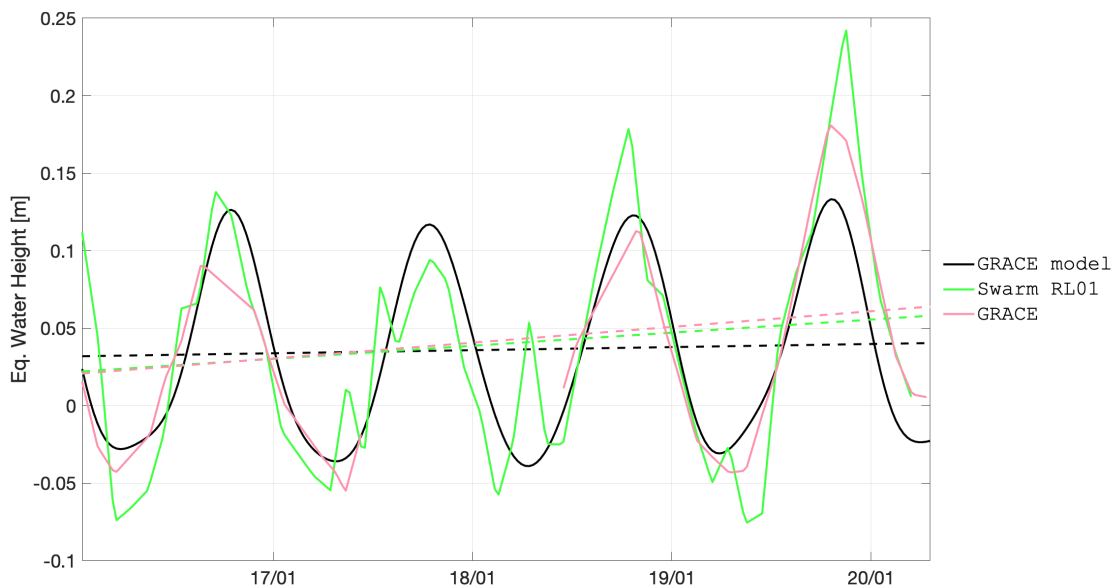


Figure 19 – Time series of EWH for the Eastern Sub-Saharan basin (latitude 1 to 13 degrees, longitude -8 to 35 degrees).

solution	constant term [cm]	constant term Δ [cm]	linear term [cm/year]	linear term Δ [cm/year]	corr. coeff. []
GRACE MODEL	3.10	0.00	0.20	0.00	1.00
Swarm RL01	3.71	0.60	0.84	0.65	0.86
GRACE	3.02	-0.08	1.02	0.82	0.91

Table 12 – Statistics of the agreement between GRACE/GRACE-FO and Swarm time series relative to the GRACE/GRACE-FO climatological model for the Eastern Sub-Saharan basin.

5.3.11 Congo and Zambezi basins

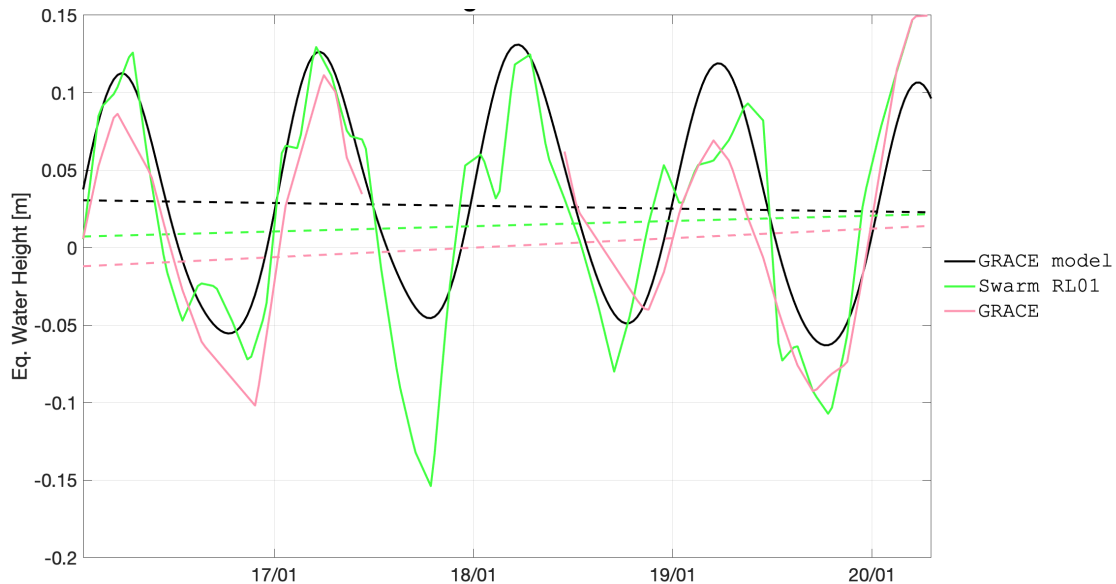


Figure 20 – Time series of EWH for the Congo and Zambezi basins (latitude -23 to -3 degrees, longitude 14 to 38 degrees).

solution	constant term [cm]	constant term Δ [cm]	linear term [cm/year]	linear term Δ [cm/year]	corr. coeff. []
GRACE MODEL	3.26	0.00	-0.18	0.00	1.00
Swarm RL01	1.84	-1.42	0.34	0.52	0.89
GRACE	1.71	-1.55	0.61	0.79	0.91

Table 13 – Statistics of the agreement between GRACE/GRACE-FO and Swarm time series relative to the GRACE/GRACE-FO climatological model for the Congo and Zambezi basins.

5.3.12 Volga basin

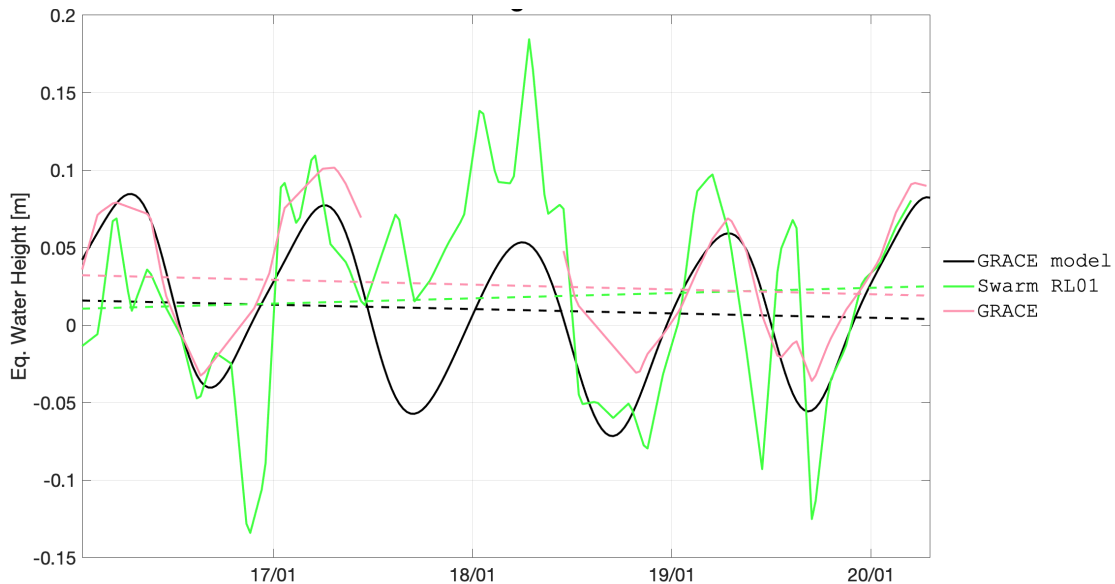


Figure 21 – Time series of EWH for the Volga basin (latitude 53 to 61 degrees, longitude 34 to 56 degrees).

solution	constant term [cm]	constant term Δ [cm]	linear term [cm/year]	linear term Δ [cm/year]	corr. coeff. []
GRACE MODEL	1.41	0.00	-0.28	0.00	1.00
Swarm RL01	2.10	0.69	0.34	0.62	0.52
GRACE	3.45	2.04	-0.31	-0.03	0.92

Table 14 – Statistics of the agreement between GRACE/GRACE-FO and Swarm time series relative to the GRACE/GRACE-FO climatological model for the Volga basin.

5.3.13 Siberia region

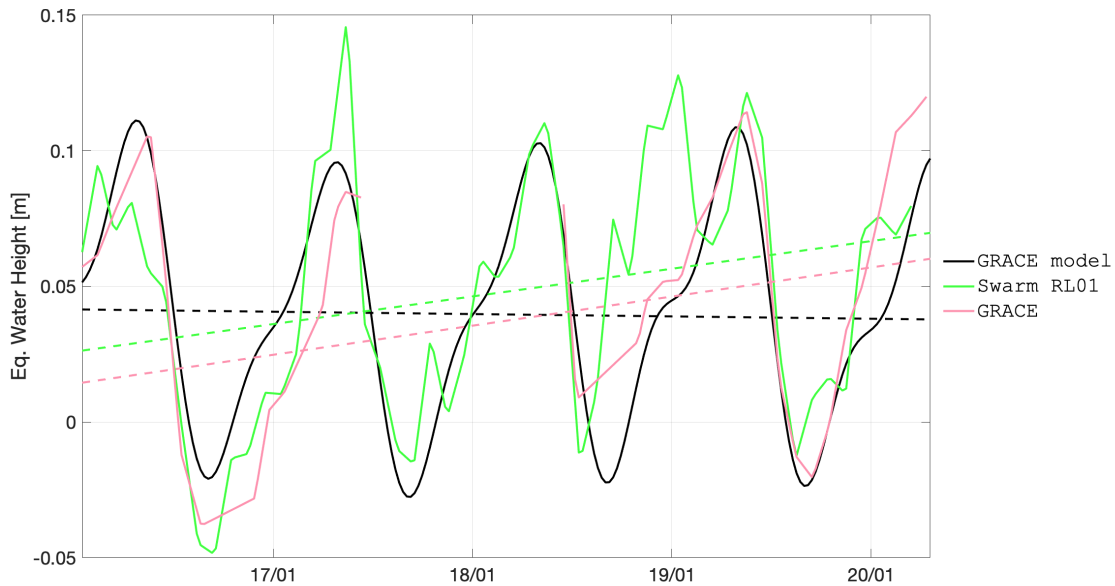


Figure 22 – Time series of EWH for the Siberia region (latitude 57 to 72 degrees, longitude 68 to 109 degrees).

solution	constant term [cm]	constant term Δ [cm]	linear term [cm/year]	linear term Δ [cm/year]	corr. coeff. []
GRACE MODEL	4.34	0.00	-0.09	0.00	1.00
Swarm RL01	4.88	0.55	1.02	1.11	0.75
GRACE	5.14	0.80	1.07	1.16	0.85

Table 15 – Statistics of the agreement between GRACE/GRACE-FO and Swarm time series relative to the GRACE/GRACE-FO climatological model for the Siberia region.

5.3.14 Ganges-Brahmaputra basin

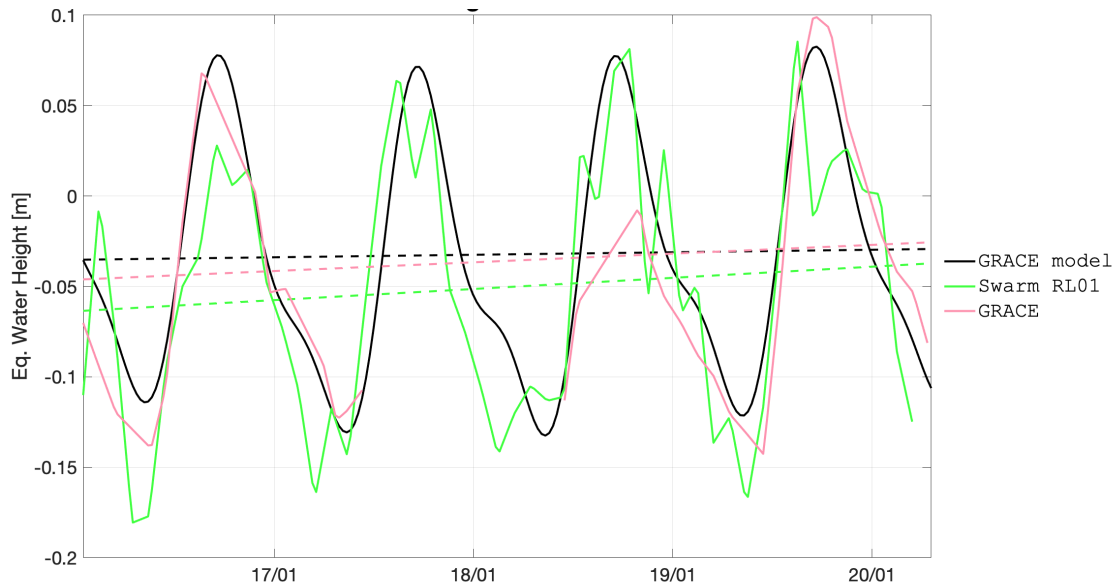


Figure 23 – Time series of EWH for the Ganges-Brahmaputra basin (latitude 15 to 30 degrees, longitude 72 to 89 degrees).

solution	constant term [cm]	constant term Δ [cm]	linear term [cm/year]	linear term Δ [cm/year]	corr. coeff. []
GRACE MODEL	-3.82	0.00	0.14	0.00	1.00
Swarm RL01	-5.31	-1.49	0.62	0.48	0.87
GRACE	-5.41	-1.60	0.48	0.34	0.89

Table 16 – Statistics of the agreement between GRACE/GRACE-FO and Swarm time series relative to the GRACE/GRACE-FO climatological model for the Ganges-Brahmaputra basin.

5.3.15 Indochina region

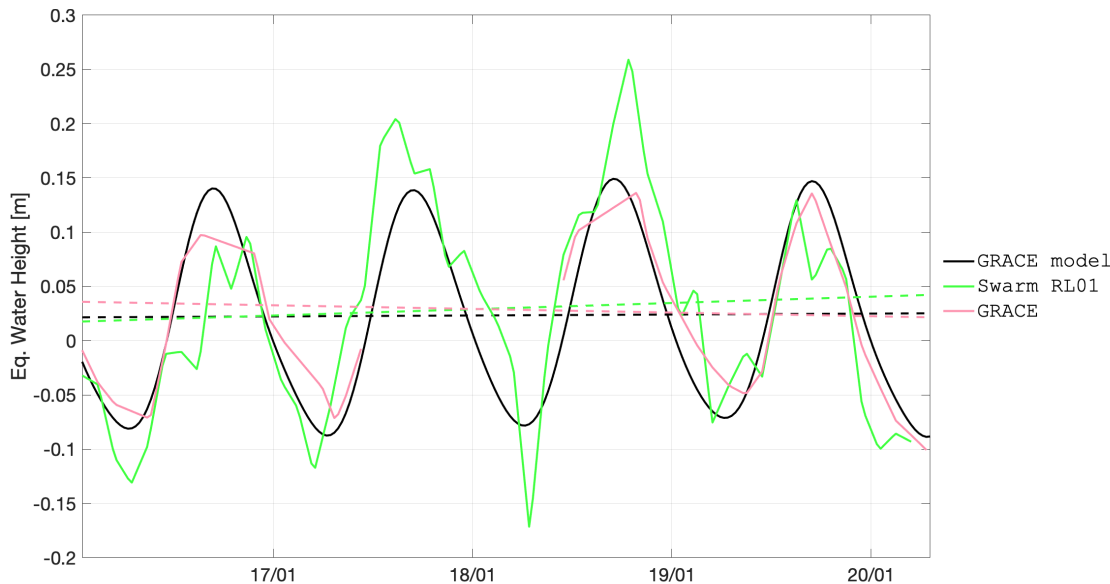


Figure 24 – Time series of EWH for the Indochina region (latitude 12 to 29 degrees, longitude 93 to 105 degrees).

solution	constant term [cm]	constant term Δ [cm]	linear term [cm/year]	linear term Δ [cm/year]	corr. coeff. []
GRACE MODEL	1.57	0.00	0.09	0.00	1.00
Swarm RL01	2.48	0.91	0.58	0.49	0.81
GRACE	1.00	-0.56	-0.34	-0.42	0.95

Table 17 – Statistics of the agreement between GRACE/GRACE-FO and Swarm time series relative to the GRACE/GRACE-FO climatological model for the Indochina region.

5.3.16 Northern Australia region

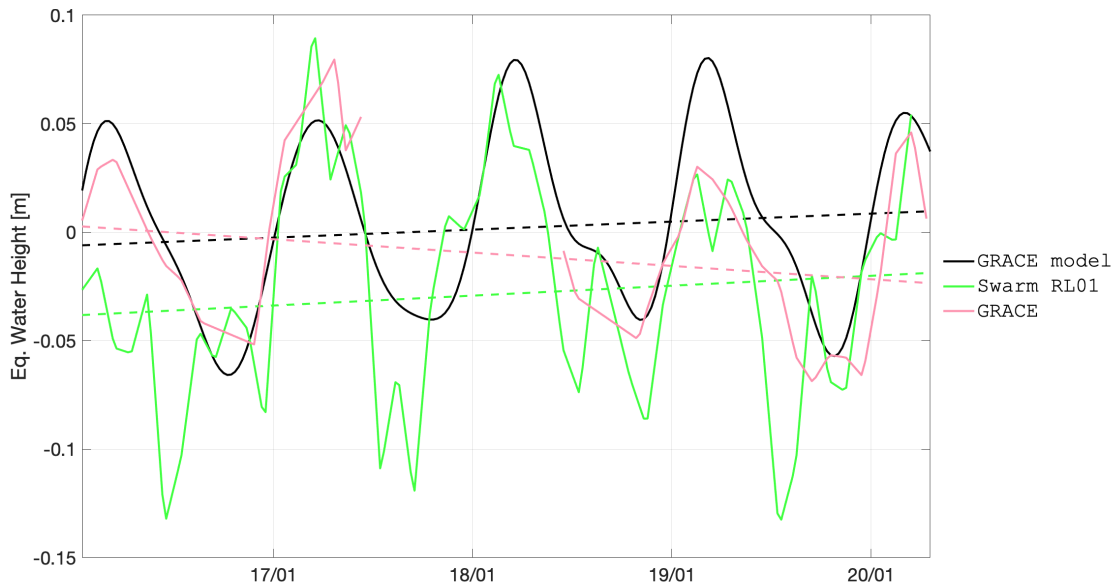


Figure 25 – Time series of EWH for the Northern Australia region (latitude -24 to -10 degrees, longitude 124 to 145 degrees).

solution	constant term [cm]	constant term Δ [cm]	linear term [cm/year]	linear term Δ [cm/year]	corr. coeff. []
GRACE MODEL	0.57	0.00	0.37	0.00	1.00
Swarm RL01	-2.58	-3.15	0.46	0.09	0.65
GRACE	-0.40	-0.97	-0.61	-0.98	0.85

Table 18 – Statistics of the agreement between GRACE/GRACE-FO and Swarm time series relative to the GRACE/GRACE-FO climatological model for the Northern Australia region.

5.3.17 Western Antarctica region

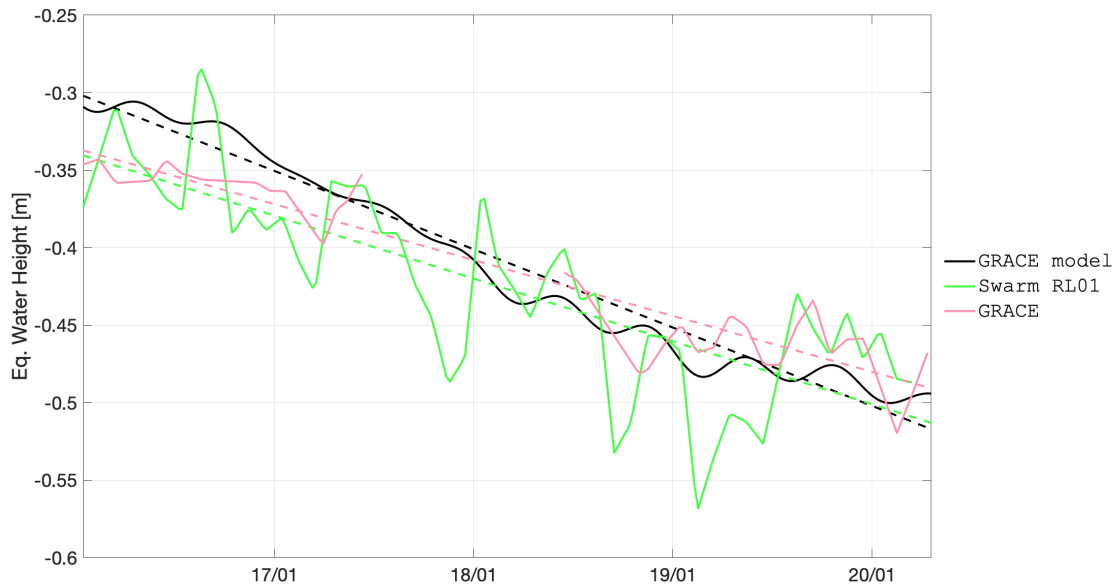


Figure 26 – Time series of EWH for the Western Antarctica region (latitude -80 to -70 degrees, longitude -140 to -85 degrees).

solution	constant term [cm]	constant term Δ [cm]	linear term [cm/year]	linear term Δ [cm/year]	corr. coeff. []
GRACE MODEL	-41.34	0.00	-5.06	0.00	1.00
Swarm RL01	-42.51	-1.17	-4.06	1.00	0.85
GRACE	-42.17	-0.83	-3.61	1.45	0.97

Table 19 – Statistics of the agreement between GRACE/GRACE-FO and Swarm time series relative to the GRACE/GRACE-FO climatological model for the Western Antarctica region.

5.3.18 Eastern Antarctica region

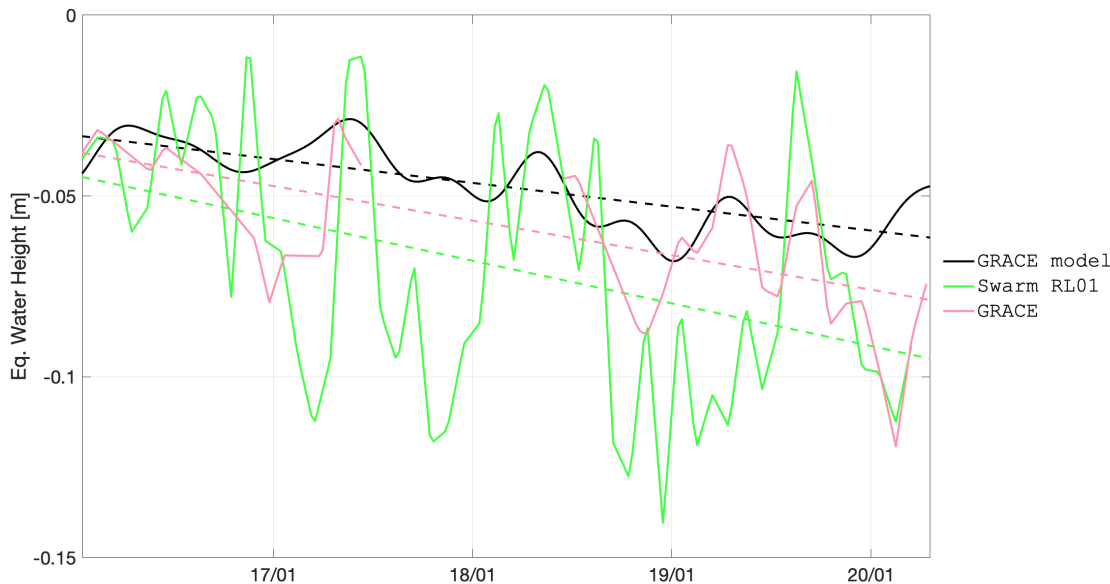


Figure 27 – Time series of EWH for the Eastern Antarctica region (latitude -80 to -68 degrees, longitude 80 to 130 degrees).

solution	constant term [cm]	constant term Δ [cm]	linear term [cm/year]	linear term Δ [cm/year]	corr. coeff. []
GRACE MODEL	-4.76	0.00	-0.66	0.00	1.00
Swarm RL01	-6.99	-2.24	-1.18	-0.52	0.48
GRACE	-6.08	-1.32	-0.96	-0.30	0.62

Table 20 – Statistics of the agreement between GRACE/GRACE-FO and Swarm time series relative to the GRACE/GRACE-FO climatological model for the Eastern Antarctica region.

5.3.19 Overview

solution	constant term Δ RMS [cm]	linear term Δ RMS [cm/year]	corr. coeff. mean []
GRACE model	0.00	0.00	1.00
Swarm RL01	1.84	0.89	0.73
GRACE	1.36	1.00	0.86

Table 21 – Statistics of the agreement between the GRACE and Swarm time series for the regions displayed in Sections 5.3.1 to 5.3.18.

5.4 Temporal variability

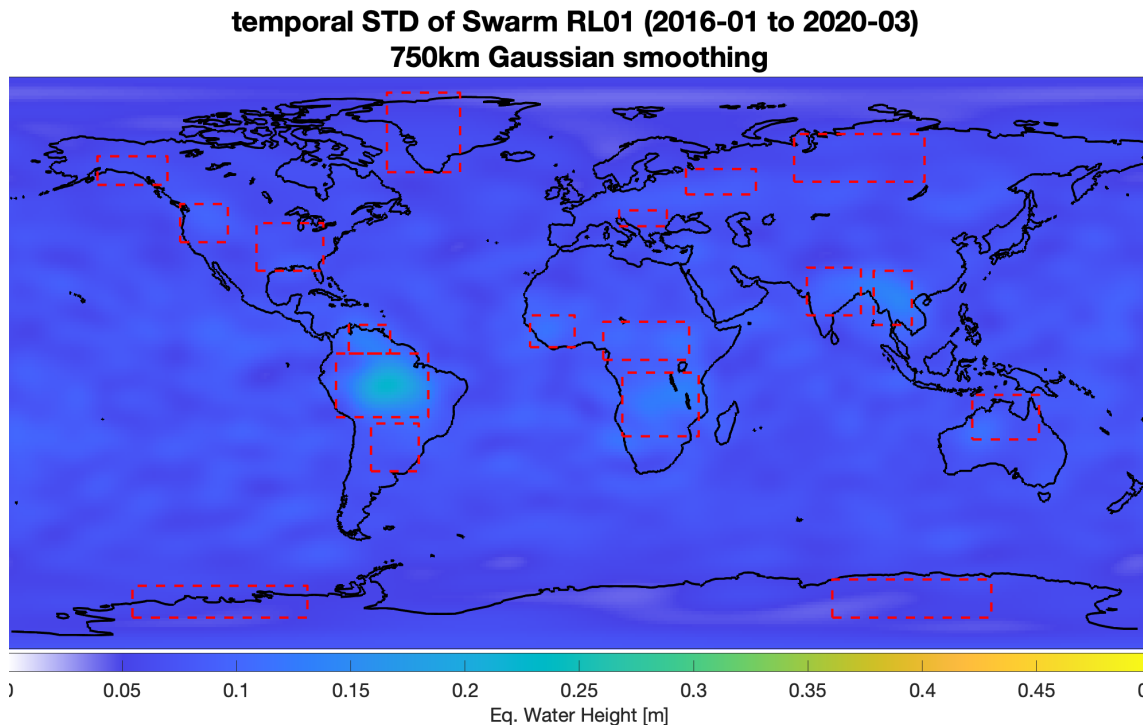


Figure 28 – Temporal variability of the Swarm combined solutions and

Acronyms

AA	Acceleration Approach, Rummel (1979)
AIUB	Astronomical Institute of the University of Bern, Switzerland, www.aiub.unibe.ch
ASU	Astronomical Institute (Astronomický ústav), AVCR, Ondřejov, www.asu.cas.cz/en
AVCR	Czech Academy of Sciences (Akademie věd České Republiky), Czech Republic, www.avcr.cz/en/
CMA	Celestial Mechanics Approach, Beutler et al. (2010)

CSR	Center for Space Research, UT Austin, USA, www.csr.utexas.edu
DAA	Decorrelated Acceleration Approach, Bezděk et al. (2014) and Bezděk et al. (2016)
EBA	Energy Balance Approach, O'Keefe (1957) and Jekeli (1999)
EWH	Equivalent Water Height
GFM	Gravity Field Model
GOCE	Gravity field and steady-state Ocean Circulation Explorer, Balmino et al. (1999) and Floberghagen et al. (2011)
GRACE	Gravity Recovery And Climate Experiment, Tapley, Reigber and Melbourne (1996) and Tapley (2004)
GRACE-FO	GRACE Follow On, Kornfeld et al. (2019)
GSFC	Goddard Space Flight Center, United States of America (USA), www.nasa.gov/centers/goddard
IEBA	Improved Energy Balance Approach, Shang et al. (2015)
IfG	Institute of Geodesy, TUG, Graz, www.ifg.tugraz.at
KO	Kinematic Orbit
N/A	Not Applicable
NEQ	Normal Equation
OSU	Ohio State University, www.osu.edu
RL06	Release 6
RMS	Root Mean Squared
SAA	Short-Arcs Approach, Mayer-Gürr (2006)
SH	Spherical Harmonic
SLR	Satellite Laser Ranging, Smith and Turcotte (1993) and Combrinck (2010)
TU Delft	Delft University of Technology, Netherlands, www.tudelft.nl
TUG	Graz University of Technology, Austria, www.tugraz.at
UT Austin	University of Texas at Austin, www.utexas.edu
USA	United States of America
VCE	Variance Component Estimation
WP	Work Package

Symbols

C Stokes coefficient.

References

- Balmino, G. et al. (1999). **The Four Candidate Earth Explorer Core Missions - Gravity Field and Steady-State Ocean Circulation Mission.** Tech. rep. SP- 1233(1). Noordwijk, The Netherlands: European Space Agency (cit. on p. 34).
- Bettadpur, Srinivas et al. (2015). **Evaluation of the GGM05 Mean Earth Gravity Model.** In: *EGU General Assembly Conference Abstracts* 17, p. 4153 (cit. on p. 6).
- Beutler, Gerhard et al. (2010). **The celestial mechanics approach: theoretical foundations.** In: *Journal of Geodesy* 84.10, pp. 605–624. DOI: 10.1007/s00190-010-0401-7 (cit. on pp. 5, 33).
- Bezděk, Aleš et al. (2014). **Gravity field models from kinematic orbits of CHAMP, GRACE and GOCE satellites.** In: *Advances in Space Research* 53.3, pp. 412–429. DOI: 10.1016/j.asr.2013.11.031 (cit. on pp. 5, 34).

- Bezděk, Aleš et al. (2016). **Time-variable gravity fields derived from GPS tracking of Swarm.** In: *Geophysical Journal International* 205.3, pp. 1665–1669. DOI: 10.1093/gji/ggw094 (cit. on pp. 5, 34).
- Cheng, M. and John Ries (2018). **GRACE Technical Note 11: Monthly estimates of C20 from 5 satellites based on GRACE RL06 models.** Austin, USA. URL: https://podaac-tools.jpl.nasa.gov/drive/files/allData/grace/docs/TN-11_C20_SLR.txt (cit. on p. 7).
- Combrinck, Ludwig (2010). **Satellite Laser Ranging.** In: *Sciences of Geodesy - I*. Ed. by Guochang Xu. Berlin, Heidelberg: Springer Berlin Heidelberg. Chap. 9, pp. 301–338. DOI: 10.1007/978-3-642-11741-1_9 (cit. on p. 34).
- Floberghagen, Rune et al. (2011). **Mission design, operation and exploitation of the gravity field and steady-state ocean circulation explorer mission.** In: *Journal of Geodesy* 85.11, pp. 749–758. DOI: 10.1007/s00190-011-0498-3 (cit. on p. 34).
- Guo, J. Y., X. J. Duan and C. K. Shum (2010). **Non-isotropic Gaussian smoothing and leakage reduction for determining mass changes over land and ocean using GRACE data.** In: *Geophysical Journal International* 181.1, pp. 290–302. DOI: 10.1111/j.1365-246X.2010.04534.x (cit. on p. 7).
- Guo, J. Y. et al. (2015). **On the energy integral formulation of gravitational potential differences from satellite-to-satellite tracking.** In: *Celestial Mechanics and Dynamical Astronomy* 121.4, pp. 415–429. DOI: 10.1007/s10569-015-9610-y (cit. on p. 5).
- Jäggi, A. et al. (2016). **Swarm kinematic orbits and gravity fields from 18 months of GPS data.** In: *Advances in Space Research* 57.1, pp. 218–233. DOI: 10.1016/j.asr.2015.10.035 (cit. on p. 5).
- Jekeli, Christopher (1999). **The determination of gravitational potential differences from satellite-to-satellite tracking.** In: *Celestial Mechanics and Dynamical Astronomy* 75.2, pp. 85–101. DOI: 10.1023/A:1008313405488 (cit. on p. 34).
- Kornfeld, Richard P. et al. (2019). **GRACE-FO: The Gravity Recovery and Climate Experiment Follow-On Mission.** In: *Journal of Spacecraft and Rockets* 56.3, pp. 931–951. DOI: 10.2514/1.A34326 (cit. on p. 34).
- Loomis, B. D., K. E. Rachlin and S. B. Luthcke (2019). **Improved Earth Oblateness Rate Reveals Increased Ice Sheet Losses and Mass-Driven Sea Level Rise.** In: *Geophysical Research Letters* 46.12, pp. 6910–6917. DOI: 10.1029/2019GL082929 (cit. on pp. 6, 7).
- Loomis, B.D. and K.E. Rachlin (2020). **GRACE Technical Note 14: NASA GSFC SLR C20 and C30 solutions.** Greenbelt, USA. URL: https://podaac-tools.jpl.nasa.gov/drive/files/allData/gracefo/docs/TN-14_C30_C20_GSFC_SLR.txt (cit. on p. 7).
- Mayer-Gürr, Torsten (2006). **Gravitationsfeldbestimmung aus der Analyse kurzer Bahnbögen am Beispiel der Satellitenmissionen CHAMP und GRACE.** PhD thesis. Rheinischen Friedrich-Wilhelms Universität Bonn. URL: <http://hss.ulb.uni-bonn.de/2006/0904/0904.pdf> (cit. on pp. 5, 34).
- O'Keefe, John A. (1957). **An application of Jacobi's integral to the motion of an earth satellite.** In: *The Astronomical Journal* 62, p. 265. DOI: 10.1086/107530 (cit. on p. 34).
- Rummel, R. (1979). **Determination of short-wavelength components of the gravity field from satellite-to-satellite tracking or satellite gradiometry.** In: *Manuscripta Geodaetica* 4.2, pp. 107–148 (cit. on p. 33).
- Shang, Kun et al. (2015). **GRACE time-variable gravity field recovery using an improved energy balance approach.** In: *Geophysical Journal International* 203.3, pp. 1773–1786. DOI: 10.1093/gji/ggv392 (cit. on pp. 5, 34).
- Smith, David E. and Donald L. Turcotte (1993). **Millimeter Accuracy Satellite Laser Ranging: a Review.** In: *Contributions of Space Geodesy to Geodynamics: Technology*. Ed. by John J.

- Degnan. Vol. 25. Geodynamics Series. Washington, D. C.: American Geophysical Union. DOI: 10.1029/GD025p0133 (cit. on p. 34).
- Tapley, B., C. Reigber and W Melbourne (1996). **Gravity Recovery And Climate Experiment (GRACE) mission.** Baltimore, USA (cit. on p. 34).
- Tapley, Byron D. (2004). **GRACE Measurements of Mass Variability in the Earth System.** In: *Science* 305.5683, pp. 503–505. DOI: 10.1126/science.1099192 (cit. on p. 34).
- Teixeira da Encarnação, João and Pieter Visser (2017). **TN-01 : Standards and Background Models.** Tech. rep. Delft, the Netherlands: Delft University of Technology. DOI: 10.13140/RG.2.2.12840.32006/1 (cit. on p. 5).
- (2019). **TN-03: Swarm models validation.** Tech. rep. TU Delft. DOI: 10.13140/RG.2.2.33313.76640 (cit. on pp. 5, 6).
- Zehentner, Norbert and Torsten Mayer-Gürr (2016). **Precise orbit determination based on raw GPS measurements.** In: *Journal of Geodesy* 90.3, pp. 275–286. DOI: 10.1007/s00190-015-0872-7 (cit. on p. 5).